Studies of Premixed Flame Propagation in Explosion Tubes

M. FAIRWEATHER,* G. K. HARGRAVE, S. S. IBRAHIM, AND D. G. WALKER
BG Technology, Gas Research and Technology Centre, Loughborough LE11 3GR, United Kingdom

An experimental and theoretical study of premixed flame propagation in a number of small-scale, cylindrical vessels is described. The study provides further understanding of flame propagation and the generation of overpressure in explosions, and allows the assessment of a mathematical model of explosions through comparisons with the experimental data obtained. Laser sheet images and data gathered on flame location, shape, and overpressures generated during the course of explosions in an empty vessel and obstacle-containing enclosures elucidate the dynamics of the various combustion processes occurring in the different chambers of the vessels. In particular, flame propagation through the vessels, up until flame front venting, is found to be substantially laminar, with significant overpressure only being generated in the later stages of explosions due to rapid turbulent combustion in the shear layers and recirculation zones induced by the obstacles. Comparisons between measurements and predictions also demonstrate that the mathematical model described provides a reasonable simulation of explosions within obstacle containing enclosures of the type investigated, with rapid turbulent combustion being predicted with sufficient accuracy to yield reasonable results for the overpressures generated.

NOMENCLATURE

C_μ	turbulence model constant
k	turbulence kinetic energy
K	Karlovitz flame stretch factor
l	turbulence length scale
r	radial coordinate
Re_l	turbulent Reynolds number (based on rms turbulent velocity and integral length scale)
t	time
u	burning velocity
z	axial co-ordinate

Greek Symbols

ϵ	dissipation rate of k

Subscripts

l	laminar
t	turbulent

INTRODUCTION

Consequence and risk assessments performed to ensure the safe design and operation of industrial plant require predictions of the damaging overpressures that might occur should a release of material result in an explosion. The development of predictive techniques capable of providing realistic estimates of explosion-generated overpressures remains a formidable undertaking however, primarily because of the complexity of the explosion process itself. The nature of the fuel involved, its stoichiometry, and the degree of any confinement all contribute significantly to the peak overpressures. In addition, the presence of repeated obstacles ahead of a propagating premixed flame can result in increased flame speeds, and hence increased overpressures, through both flame distortion effects and the positive feedback mechanism between flow field turbulence and burning rate. Any reliable predictive method must therefore account for all these factors, as well as contain some representation of the majority of obstacles present within the flow field, the extent to which such obstacles generate turbulence, and the way in which a propagating flame interacts with them.

Experimental studies are also required in order to further understand the physical processes which are important in the generation of overpressures, and to elucidate how these processes, and local conditions, influence the severity of an explosion. In addition, the development of control techniques capable of reducing the overpressures generated is an important area for experimental research, and the data

*Corresponding author. Address: BG Technology, Gas Research and Technology Centre, Ashby Road, Loughborough LE11 3GR, Leicestershire, England. E-mail: michael.fairweather@bgtech.ac.uk

0010-2180/99/$–see front matter
PII S0010-2180(98)00055-8

gathered from all such work is invaluable to the validation of appropriate predictive techniques.

While experimental and theoretical work on large-scale items of plant, or idealized representations thereof, continue to provide information that is useful to understanding, predicting and mitigating the effect of explosions, the complexities associated with the explosion process mean that studies in small-scale, simplified geometries are also required to develop basic understanding of the flame propagation process and to demonstrate the validity of the predictive techniques. To this end, a number of authors have described experimental studies performed in simple geometries; for example, in cylindrical chambers containing spirals of tubing [1] and in rectangular cross-sectioned tubes with flat plates orthogonal to the flow [2]. Mathematical models capable of predicting turbulent premixed flame propagation in transient compressible flows have also been described [3, 4] and validated against such data.

The present paper describes a joint experimental and theoretical study of premixed flame propagation in a number of small-scale, cylindrical vessels. The main aim of this work was to elucidate the dynamics of the combustion processes occurring in the different vessels, and to investigate further how obstacle-generated turbulence leads to increased combustion rates and overpressures. The experimental data have also been used to assess the accuracy of a mathematical model of explosions described previously [5]. In addition to demonstrating the validity of the modeling approach adopted for predicting overpressures generated by rapid turbulent combustion, the study also examines the applicability of methods used to handle the transition from laminar to turbulent flame propagation that occurs in explosions in many idealized and practically relevant geometries. The work complements previous experimental studies in closed cylindrical vessels both with [6, 7] and without [6] a single orifice plate, and in a vented tube containing 12 obstacle rings [8]. It also extends earlier experimental [9] and theoretical [5, 9] work by the present authors to encompass explosions in a range of small-scale vessels, to consider detailed observations of the combustion process, and to validate further the mathematical modeling approach adopted over a wider range of explosion conditions.

EXPERIMENTAL WORK

Three cylindrical vessels were constructed from 6-mm-thick Perspex tubes to provide optical access, each with an internal diameter of 288 mm. The tubes were fitted with 20-mm-thick flanges at both ends, with the flange at the closed, lower end of the tubes containing fittings for a spark igniter, fuel–air inlet, gas sample line, seeding system and pressure transducer, while the top flange contained a vent opening and fittings for fuel–air outlet, sample line, and pressure transducer. The spark igniter was mounted at the center of the lower flange. The first vessel employed (Vessel A) had a length to diameter ratio of 3, contained no turbulence-inducing rings, and had a flange at the vent opening with an area blockage of 75%. The second vessel (Vessel B) had a length to diameter ratio of 2, and contained a single, 6-mm-thick turbulence-inducing ring located one diameter along its length. The area blockage of the internal ring was 33%, while that of the flange at the vent opening was 75%. The third vessel (Vessel C) had a length to diameter ratio of 3, contained two internal rings located at 1 and 2 tube diameters, and both the internal baffles and the vent opening had an area blockage of 50%. All the vessels were orientated vertically, with the tube held between two 6-mm-thick steel flanges with rubber seals between the flanges and the tube. The flanges at either end of the tube were mounted onto a steel support using adjustable clamps. A schematic diagram of Vessel C is given in Fig. 1.

During gas filling, the open end of the vessels was covered by a thin plastic membrane that was sealed to the flange using silicone grease, giving a failure pressure of approximately 10 mbar. The vessels were filled by purging with a premixed methane–air mixture, with air from a compressor and methane (99.5% by volume) from a high-pressure cylinder. Mixture within the vessels was continuously withdrawn during the filling sequence, via the sample ports, and monitored using an infrared analyzer. In all the experiments reported, stoichiometric mixtures

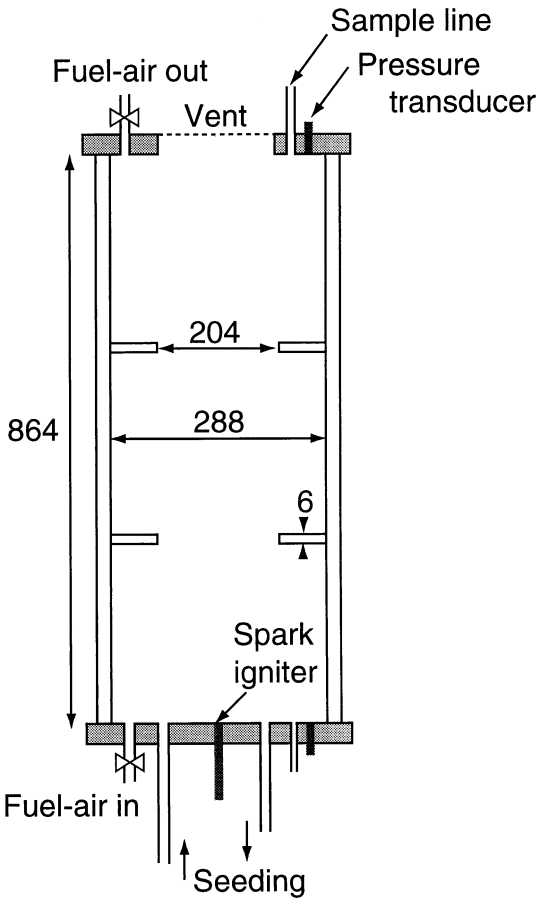

Fig. 1. Schematic diagram of Vessel C (all dimensions in mm).

of methane (9.5 ± 0.1%) and air were used. Laser sheet images were obtained by seeding with ultrafine (0.05-μm-diameter) aluminium oxide particles as part of the filling sequence. A short time delay (approximately 5 s) following seeding was incorporated into the filling sequence before firing, in order to allow the gas mixture to become essentially quiescent while maintaining the seed in suspension. Ignition and data capture were automatically sequenced by a timer control unit. The flammable mixture was ignited by an electrical spark produced by discharging a 32-μF capacitor charged to 160 V through the primary windings of a car ignition coil, with the secondary windings connected to the spark electrode.

During testing, pressure–time histories at the closed and vent ends of the vessel were obtained using transducers located at a radial distance of 0.115 m from the vessel axis. Output from the transducers was amplified and recorded at a sampling rate of 500 kHz. Flame propagation was recorded using a high-speed video camera system, with laser sheet images derived using the same system in conjunction with a 30-W copper vapor laser (pulse width 30 ns), the pulses of which were synchronized to the video camera framing rate. After a number of test experiments to establish the optimal combination of temporal and spatial resolution and image quality, a framing rate of 4500 frames per second was chosen.

Repeat tests were performed to demonstrate reproducibility and to allow the derivation of ensemble-averaged pressure data for those cases with significant turbulence effects. Reproducibility between all tests was found to be good, with peak pressures varying by less than ±5% in magnitude. Flame arrival times and the time of occurrence of peak pressures were also found to be reproducible, with typical variations of ±5 ms in 100 ms. These small time differences between tests may be attributed to small (<2%) variations in equivalence ratio, and to changes in the development of the initial flame kernel and subsequent early stages of the laminar flame propagation phase. These in turn led to small time displacements of the pressure–time records between tests which were removed, prior to averaging, by converting the time scale of an individual test to an average value by introducing an offset in the time scale of the individual test. Ensemble-averaged information was derived from data obtained in at least three trials [2, 10]. This approach minimized contributions from what are conventionally thought of as "cycle-to-cycle" variations between tests. Flame shapes, obtained prior to venting from the tube, were essentially identical once these time shifts, to synchronize flame arrival times along the centerline of the tube, had been implemented. In the results discussed below however, flame shapes are given for a single test representative of the mean.

MATHEMATICAL MODEL

The mathematical model used is described elsewhere [5, 9], with only brief details being given

below. Predictions were based on solutions of the ensemble-averaged, density-weighted forms of the transport equations for mass, momentum, total energy, and a reaction progress variable. Closure of this equation set was achieved using the standard [11] form of the k-ϵ turbulence model, modified to include compressibility effects [12]. Effective viscosities which contained both laminar and turbulent contributions were used throughout, with conventional forms of the conservation equations together with standard values of modeling constants [11].

Turbulent premixed combustion was accommodated in these equations by modifying the turbulent diffusion coefficients and source terms used in the conservation equations for total energy and the reaction progress variable in a way which ensured that numerical solutions gave rise to a flame that reproduced a specified turbulent burning velocity. This was achieved by applying a reaction rate model based on the eigen value analysis of Catlin and Lindstedt [13] which incorporates both chemical kinetic and flow field influences on the burning velocity of a flame, and also maintains realistic flame thicknesses throughout the course of an explosion. Essentially, a modified form of the eddy breakup reaction rate expression was used in which reactants produce products via a single-step irreversible reaction, with the variation of reaction rate through the flame prescribed by a power law expression which eliminates the cold front quenching problem [14] and provides a realistic heat release rate profile across the reaction zone. Turbulent diffusion coefficients and source terms in the energy and progress variable transport equations required to reproduce a given turbulent burning velocity were then specified, within the diffusion-reaction zone of the flame, from a known flame thickness and eigen values determined from one-dimensional calculations of planar flame propagation. Flame thickness was equal to a turbulence length scale derived from the k-ϵ model, namely $l = C_\mu^{3/4} k^{3/2}/\epsilon$, which in turn ensured adequate numerical resolution of the flame front. Turbulent burning velocities were obtained from known mixture and calculated flow field parameters via the expressions of Gülder [15] and, outside the range of applicability of the latter, from that of Bray [16]. Flame quenching, caused by high levels of flow field turbulence, was also implemented within the combustion model using the criteria proposed by Poinsot et al. [17]. Modeling constants were assigned standard values consistent with the assumptions of unity Lewis number and an isentropic index of 1.4.

Solutions to the time-dependent, axisymmetric forms of the descriptive equations were obtained using a modified version of a general purpose fluid dynamics code. Within the code, integration was performed using an explicit, second-order accurate, finite-volume scheme. Diffusion and source terms in the modeled equations were approximated using central differencing, while approximations to convective and pressure fluxes were derived using a second-order accurate variant of Godunov's method. The calculations also employed an adaptive finite-volume grid algorithm which used a two-dimensional, rectangular mesh, with grid adaption by overlaying successively refined layers of computational mesh. Each layer was generated from its predecessor by doubling the number of computational cells in each space direction. This technique allowed the generation of fine grids in regions of high spatial and temporal variation and, conversely, relatively coarse grids where the flow field was smooth. In the calculations reported below up to six layers of mesh (corresponding to a minimum cell size of 1.2 mm) were used in deriving grid-independent solutions, with the aspect ratio of the cells being one at all times. Computed arrival times of flame along the centerline of Vessel C are given in Fig. 2, which illustrates that grid-independent solutions were effectively achieved using six grid layers. Predictions of pressures within the various vessels similarly required six levels of mesh to resolve adequately the turbulent shear layers and recirculation zones and to yield converged results.

In the computations, the centerline of the explosion tube, represented by the z-axis at $r = 0$, was taken as a symmetry boundary and no-slip conditions were imposed along the walls of the tube and internal obstacles, with finite-volume solutions patched onto fully turbulent, local equilibrium wall law profiles. The remaining boundaries, outside the tube, were taken as outflow surfaces, with sensitivity studies demonstrating that at the locations used for these

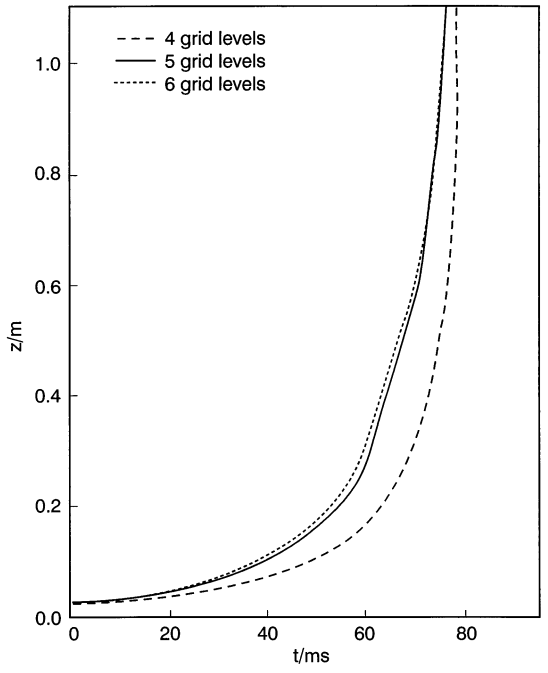

Fig. 2. Influence of grid refinement on predicted time of arrival of flame on centerline of Vessel C.

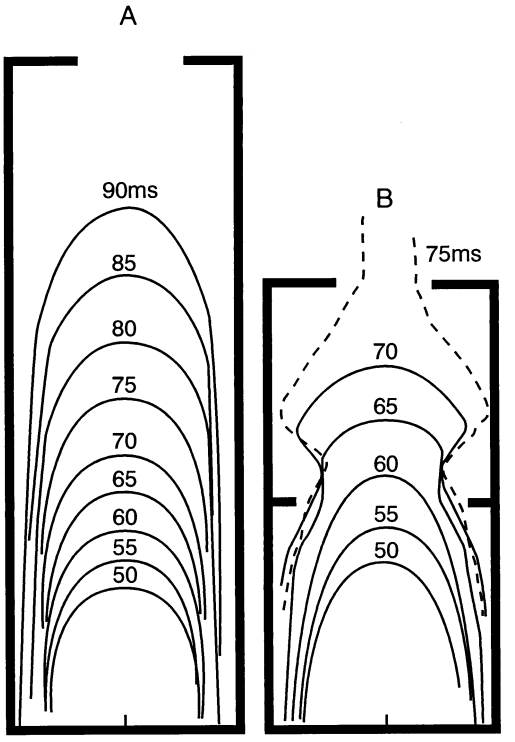

Fig. 3. Observed flame shapes during explosion in Vessels A and B.

surfaces the boundary conditions enforced there exerted a negligible influence on all the results. Ignition was initiated by prescribing the equivalent of a hemispherical region of burned gas, with a radius of 0.025 m, at the center of the closed end of the vessel, with velocities throughout the tube being set to zero. In reality, initial flame propagation was laminar. Initial turbulence levels required by the k-ϵ model were therefore chosen [5] in such a way as to ensure that the turbulent burning velocity given by the expressions of Gülder [15] was close to the laminar value. As well as providing reasonably realistic initial conditions for the computations, this approach also ensured numerical stability and that the time scale associated with the decay of turbulence within the tube was long compared to the overall time of the calculations. The sensitivity of model solutions to the initial levels of turbulence employed was examined, in line with earlier work [5], and the results presented below were derived assuming an initial scale of turbulence of the same order as the Kolmogorov length scale (i.e., l = 1.2 mm).

RESULTS AND DISCUSSION

Experimental Results for Flame Propagation and Pressure Generation

Flame shapes observed during the course of explosions in Vessels A and B are given in Fig. 3. In the empty vessel the flame is seen to be symmetric about the vessel axis at all times, with the flame moving away from the ignition point with a roughly hemispherical shape and a burning velocity close to the laminar value. With increasing time, increases in flame area, and hence the rate of production of burned gas, cause the flame front to preferentially accelerate along the axis of the tube, distending towards the vent before exiting the vessel approximately 96 ms after ignition with a terminal, centerline flame speed of 44 m s^{-1}. Beyond that time, the flame within the vessel burnt smoothly towards the tube walls until combustion was completed, with the flame surface remaining laminar and continuous at all times.

Initial flame propagation in Vessel B was similar to that in Vessel A, although a comparison of flame shapes in Fig. 3 shows that the obstacle ahead of the flame started to influence its shape by 50 ms. Between 65 and 70 ms the flame front is seen to propagate towards the walls of the vessel, within the second chamber. The flame exited the vessel 74 ms after ignition with a terminal, centerline flame speed of 61 m s^{-1}. At no time was the flame front observed to be drawn into the recirculation zone located behind the internal obstacle. This may be attributed to the low blockage (33%) of the obstacle used within Vessel B, and hence the weakness of the recirculation zone created. After flame venting, the flame front again propagated towards the walls of the vessel in a smooth fashion, and as a continuous laminar flame sheet, with combustion being completed first within the vessel chamber closest to the vent. Compared with combustion in Vessel A, that within Vessel B was slightly more turbulent and, as will be seen later, gave rise to overpressures about a factor of two higher.

Frames taken from the high-speed video films are given in Fig. 4, and show flame propagation within Vessel C in more detail. Initial flame propagation is similar to that in Vessel B, although between 65 and 75 ms the flame front is seen to move in the radial direction and to be ultimately drawn into the recirculation zone generated behind the first obstacle which had a significantly higher blockage (50%) than that in Vessel B. The flame exited the explosion tube after approximately 78 ms with a terminal, centerline flame speed of 61 m s^{-1}. By 80 ms rapid turbulent combustion in the second chamber of the vessel, and slower near-laminar combustion in the first (ignition end) chamber, are seen to be almost complete. As will be seen later, significant pressure rise within the vessel only starts beyond 80 ms during the final stages of combustion in the second chamber, and as turbulent burning towards the wall of the tube begins in the third vessel chamber adjacent to the vent. At no time was the flame front observed to be drawn into the recirculation zone located behind the second internal obstacle. Combustion was completed first in the second chamber (by 88 ms), followed by the third and finally the first chamber (by 96 ms).

These observations demonstrate that turbulence-enhanced burning was greatest within the middle chamber of Vessel C. Laser sheet images obtained downstream of the first obstacle, closest to the ignition end of the tube and within the middle chamber, are given in Fig. 5. As the flame front propagates towards the first obstacle, vortices are formed from approximately 35 ms. These vortices are shed from the first obstacle, and their size increases with time as flow velocities through the vent created by the first obstacle increase due to flame acceleration effects. By 55 ms a strong recirculation zone has been established although, in line with the numerical predictions of Barr [18], this feature is not stationary (or standing) since it continues to be convected downstream. The flame front appears in the middle chamber 57 ms after ignition, by which time the recirculation zone has a length approximately twice the height of the obstacle. As the flame front (observed as a wrinkled interface between dark burned gas regions and lighter unburned regions at 60 ms in Fig. 5) continues to accelerate along the vessel centerline, the size of the recirculation zone continues to grow until it is approximately three times the obstacle height. Between 62.5 and 65 ms the flame front begins to propagate radially towards the walls of the vessel, following the flow of unburned gas, and ultimately rolls into the large-scale turbulent vortex located behind the obstacle. This can be seen in the laser sheet images where, at 70 ms, the flame front has folded on itself and is propagating upstream towards the obstacle in close proximity to the wall. By 72.5 ms the flame front has reached the center of the turbulent eddy. This induces rapid combustion, with expansion of burned mixture close to the vessel wall causing some of the unburned gas to be convected towards the vessel axis (between 72.5 and 75 ms). From Fig. 4, these events take place at a time when flame propagation along the vessel centerline has reached a point where flame enters the third vessel chamber. Breakup and fragmentation of the continuous flame sheet is observed between 72.5 and 75 ms, and as combustion continues the flame brush is seen to thicken, with unburned regions of mixture beginning to appear within the burned gases. Combustion within this

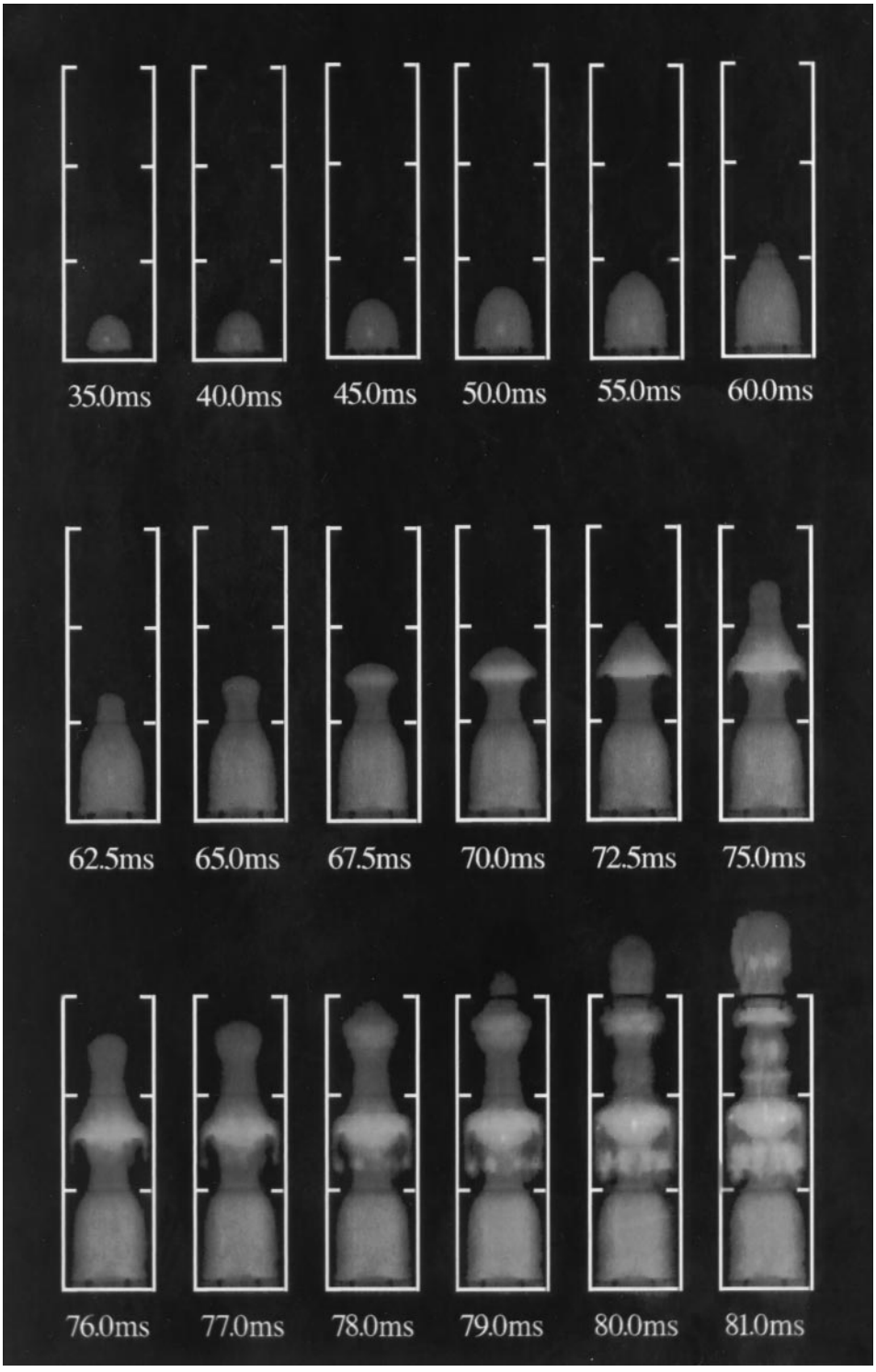

Fig. 4. Video images of flame shapes during explosion in Vessel C.

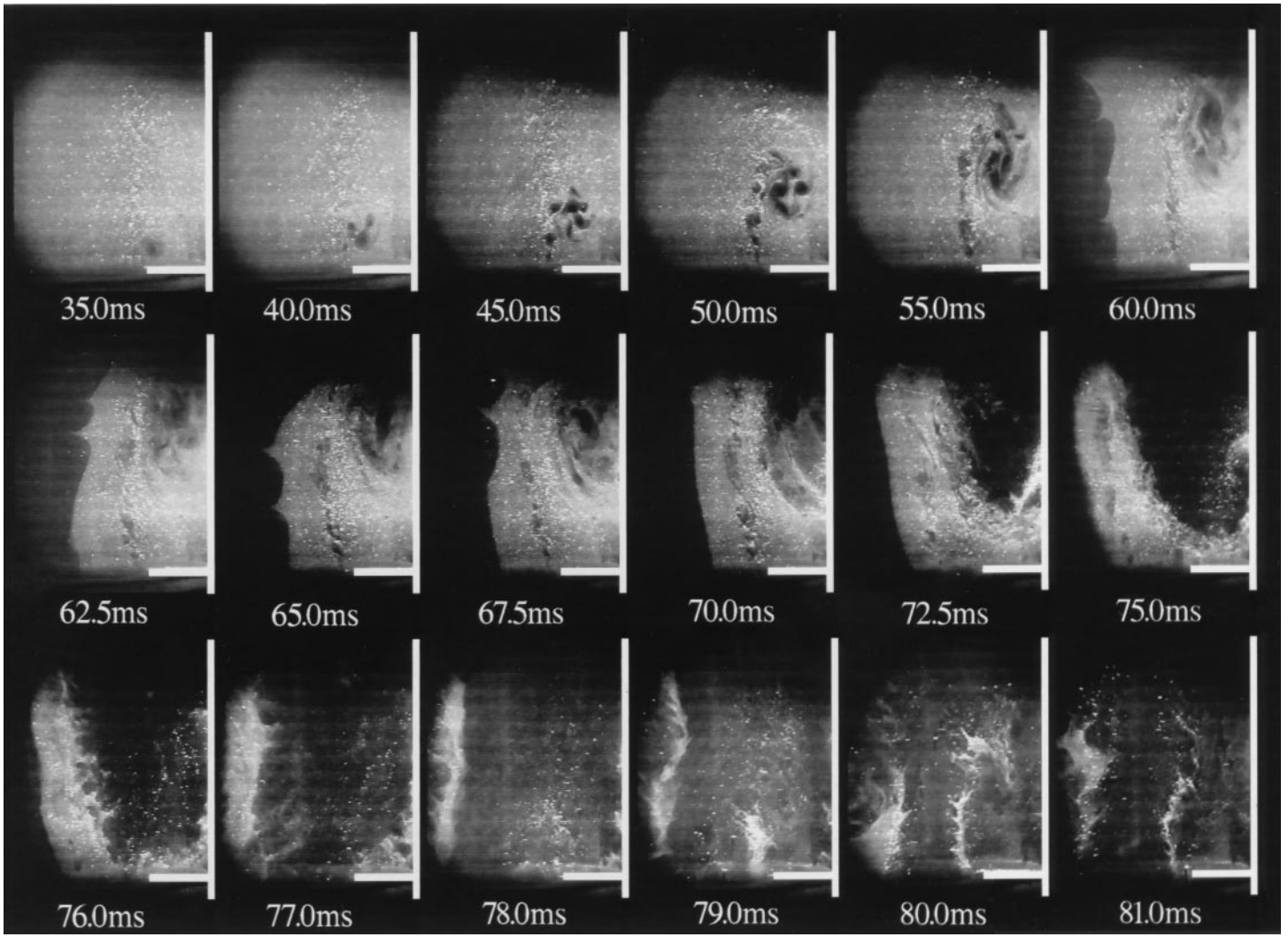

Fig. 5. Laser sheet images downstream of first obstacle in Vessel C.

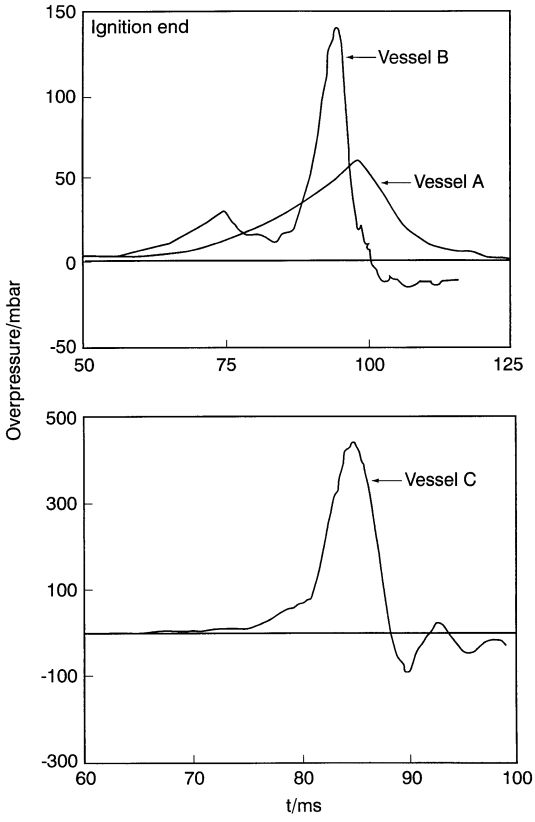

Fig. 6. Observed pressure–time profiles at ignition end of all three vessels.

region of the flow was completed by approximately 84 ms.

Pressure profiles obtained at the ignition end of the vessels are given in Fig. 6. In Vessel A, pressure rise is seen to be continuous up until the time the flame exits the vessel at 96 ms, at which point the onset of burned gas venting and flame quenching on the vessel walls leads to a reduction in internal pressures. A similar reduction in pressure within Vessel B is observed at 74 ms, again coincident with the onset of burned gas venting, with the rate of pressure rise just prior to venting being similar to that observed in Vessel A. Beyond 83 ms, however, pressure begins to rise rapidly as turbulent flame propagation into the corners of the second chamber takes place, with combustion in both chambers being effectively completed by 94 ms. Burned gas venting from Vessel C causes an inflection in the pressure profile at approximately 78 ms, with rapid pressure rise at 80 ms coinciding with the final stages of combustion in the second chamber, and as turbulent burning towards the wall of the tube begins in the third vessel chamber adjacent to the vent. The peak pressure of 450 mbar occurs at 84 ms as rapid combustion behind the first obstacle is completed, with pressure decaying as the reaction rate within the second chamber decreases and as the last vestiges of trapped unburned mixture are consumed in the ignition and vent end chambers. Data obtained at the vent end of the various vessels confirmed that almost uniform peak pressures were achieved within each vessel.

In all cases venting of flame from the vessel resulted in the ignition and combustion of a cloud of unburned mixture that had been previously ejected from the tubes. In Vessels A and B this mixture was not highly turbulent, and its combustion was relatively slow. In the case of Vessel C, however, rapid turbulent combustion of the vented unburned mixture was observed. A separate series of experiments was therefore performed using Vessel C with a flame trap over the vent of the vessel which prevented any external combustion. These experiments established that the external combustion process had little influence on the rate of pressure rise or peak pressures generated within the vessel, although pressure decay was observed to be more rapid with the flame trap in place.

Comparison of Model Predictions and Experiment

Predicted flame front locations are given in Fig. 7 for Vessels A and B, and in Fig. 8 for Vessel C. The contours given in these figures represent those locations where the computed mean reaction progress variable equaled 0.5.

In Vessel A the general shape and progress of the flame front are predicted well, although the calculated position of the flame on the centerline of the vessel tends to lag slightly behind measurements up to 60 ms. After this time the predicted flame accelerates towards the vent more rapidly than is observed, and ultimately exits the vessel well ahead of the measured flame. This is seen more clearly in Fig. 9a which compares measured and predicted times of ar-

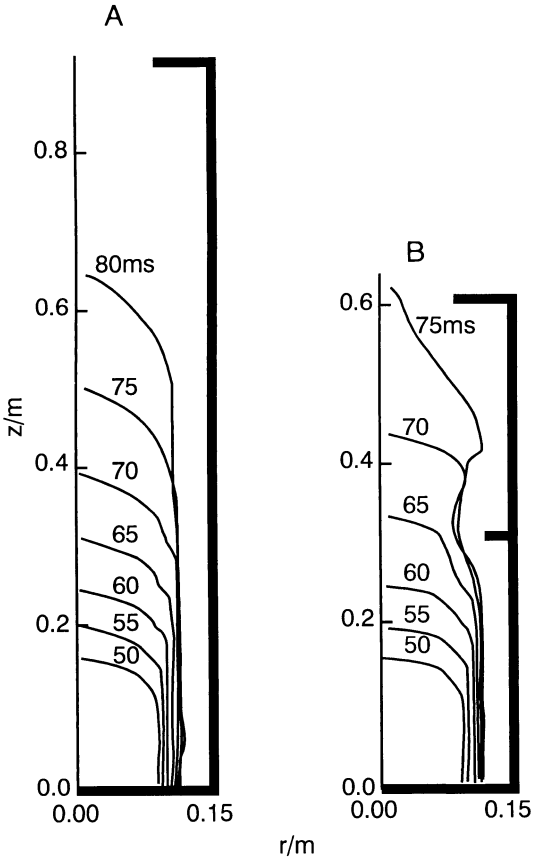

Fig. 7. Predicted flame shapes during explosion in Vessels A and B.

rival of flame along the centerline of all three vessels. This overestimation of flame speeds at later times in Vessel A may be attributed to the fact that while flame propagation within this vessel remained laminar up until combustion was completed, the predictive methodology adopted is intended for use in flow situations that become fully turbulent. Solution of the k-ϵ turbulence model therefore inevitably leads to some turbulence generation within the vessel, which in turn increases local burning velocities above the laminar value, causing an overprediction of the rate of burned gas production and flame speed. The present model, being based on a fully developed turbulent flow formulation, cannot therefore be expected to predict flame propagation and overpressure generation with Vessel A with any degree of accuracy. These comparisons between theoretical and experimental results do, however, demonstrate the validity of the approach adopted within the mathematical model for treating initial laminar flame development. As described earlier therefore, choosing initial turbulence levels in such a way as to ensure that the turbulent burning velocity given by the expressions of Gülder [15] was close to the laminar value, and consistent with an initial scale of turbulence of the same order as the Kolmogorov scale, not only provides realistic initial conditions for the computations, but ensures that the predicted flame propagates with an essentially laminar burning velocity for a significant time before turbulence generation causes deviations from measurements. Indeed, throughout combustion within Vessel A, predicted turbulence levels were sufficiently low for flame propagation to remain well within the continuous laminar flame sheet regime defined by Abdel-Gayed et al. [19], with maximum local values of $u_t/u_l = 6$, $Re_l = 300$ and $K = 0.04$ only occurring at the very end of the computations as flame burnt into the corners of the vessel. As will be seen below, provided obstacle-generated turbulence occurs sufficiently early in computations for situations where fully developed turbulent flow ultimately develops, as in most practical geometries, the modeling approach adopted allows the transition from laminar to turbulent flame propagation to be accommodated.

Comparisons between Figs. 3 and 7 for Vessel B show closer agreement between predictions and observations. In particular, from Fig. 9b, although the centerline location of the predicted flame again lags behind measurements up to approximately 60 ms, the terminal, centerline flame speed achieved and the time of flame exit from the vessel are both reproduced by the model. In addition, the predicted flame was again observed to propagate towards the walls of the vent-end chamber without being drawn into the recirculation zone located behind the internal obstacle, and after flame venting it continued to burn towards the walls of the vessel in a smooth fashion. In agreement with observations, combustion within this vessel was predicted to occur within the continuous laminar flame sheet regime [19], with maximum local values of $u_t/u_l = 14$, $Re_l = 3500$, and $K = 0.15$ occurring at the end of the computa-

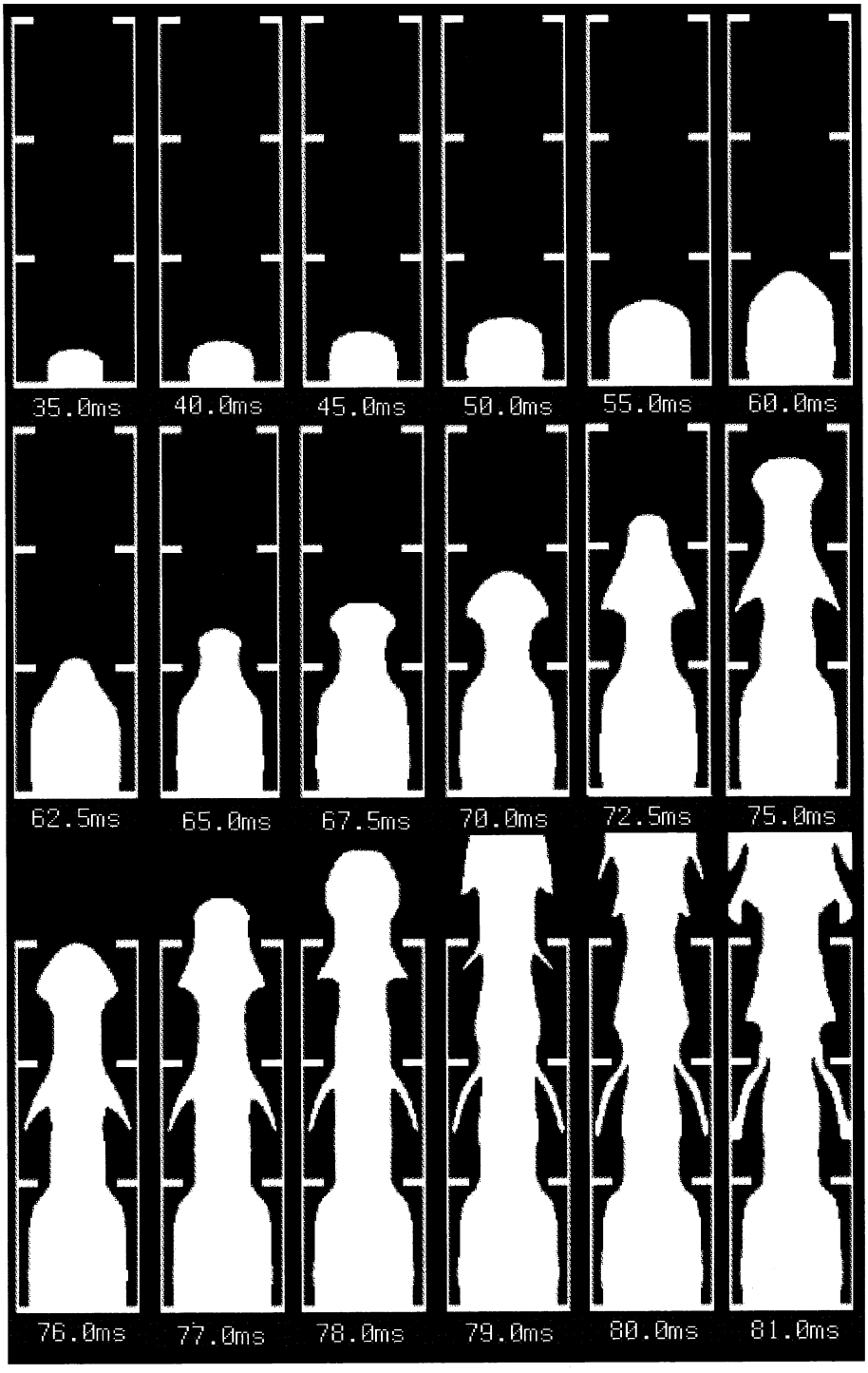

Fig. 8. Predicted flame shapes during explosion in Vessel C.

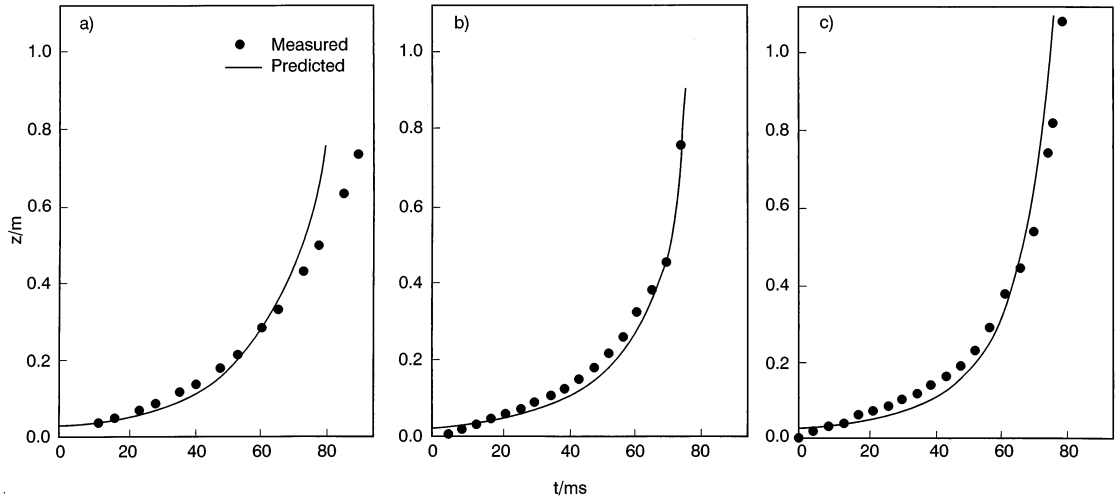

Fig. 9. Comparison of measured and predicted time of arrival of flame on centerline of (a) Vessel A, (b) Vessel B, and (c) Vessel C.

tions as the flame burnt into the corners of the vessel.

Figure 8 gives predicted flame shapes within Vessel C at equivalent times to the frames taken from the high-speed videos shown in Fig. 4. Overall, close agreement between measured and predicted results is apparent, with the predicted flame front being drawn into the recirculation zone generated behind the first obstacle, although not into that behind the second obstacle. From Fig. 9c, the predicted location of the flame front on the centerline of the vessel lags behind measurements up to 60 ms. After this time the predicted flame accelerates towards the vent more rapidly than is observed, exiting the tube at 76 ms compared to the experimental time of 78 ms. The predicted terminal, centerline flame speed is, however, seen to be in close accord with observations. Beyond 81 ms, flame within the third chamber was predicted to burn smoothly towards the walls of the vessel. Turbulence-enhanced burning was predicted to be greatest within the middle chamber, with maximum local values of $u_t/u_l = 18$, $Re_l = 6000$, and $K > 0.5$. Turbulence levels therefore indicated that combustion within this chamber extended well into the regime in which a fragmented flame, existing as a brush of burning pockets of flammable material [19], occurs. Flame quench effects, accommodated using the criteria proposed by Poinsot et al. [17], were also apparent in the computations, with earlier studies [9] indicating that this quench criterion is required in order to obtain agreement between measured and predicted mean axial velocities within this vessel. Calculations that did not incorporate such quenching effects also demonstrated that predicted overpressures were reduced slightly by the quenching process.

As remarked earlier, little is to be gained by a detailed comparison between measured and predicted overpressures generated in Vessel A, since turbulence levels towards the end of the explosion were overpredicted, causing in turn a significant overprediction of the peak pressures generated. This overprediction of turbulence levels therefore led to predicted peak overpressures of 98 and 113 mbar at the ignition and vent ends of the vessel, respectively, compared to experimental values of 62 and 66 mbar, with the predicted pressure peaks occurring at 81 ms compared to the observed value of 97 ms. Pressure profiles obtained at the ignition and vent ends of Vessels B and C are given, respectively, in Figs. 10 and 11. In Vessel B, and in agreement with earlier observations, the decrease in pressure associated with the onset of burned gas venting (at 74 ms) is correctly predicted, although beyond this time turbulent combustion within the second chamber is calculated to occur too rapidly, causing the rate of

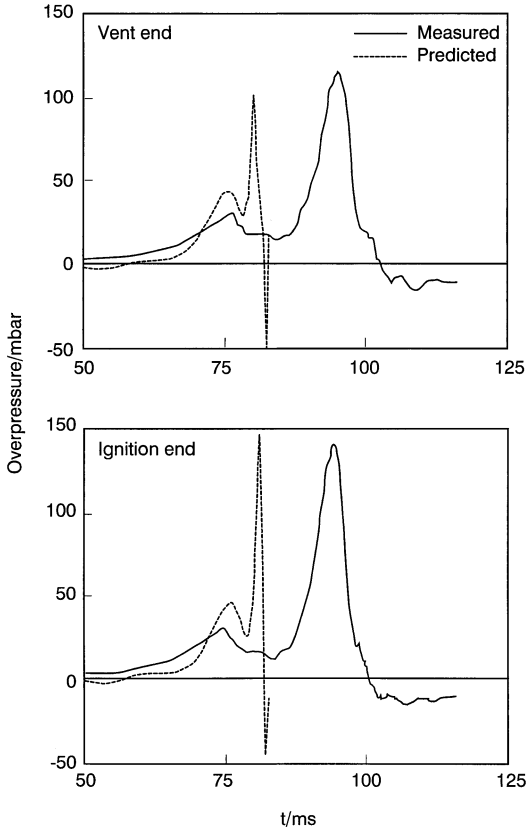

Fig. 10. Comparison of measured and predicted pressure–time profiles in Vessel B.

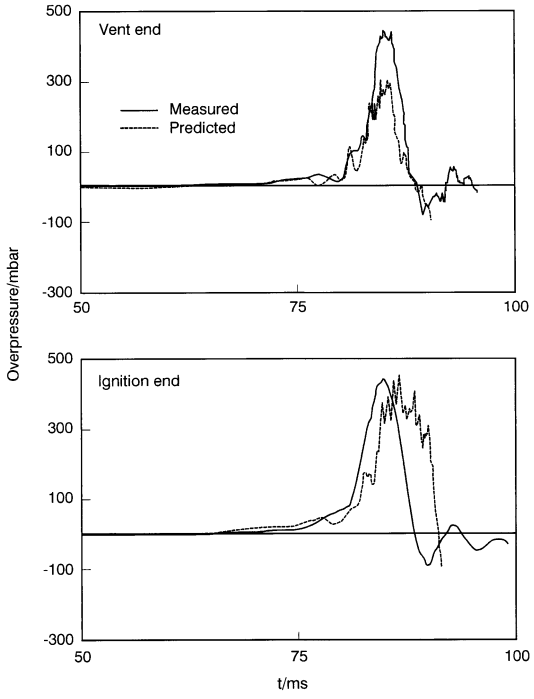

Fig. 11. Comparison of measured and predicted pressure–time profiles in Vessel C.

pressure rise to be overpredicted and the duration of the main pressure peaks to be underpredicted. The peak pressures achieved in the computations are, however, in good agreement with measured values. Burned gas venting from Vessel C causes an inflection in the measured ignition end pressure profile at approximately 78 ms, with an actual decrease in pressure being observed at the vent end of the vessel. Equivalent theoretical results predict burned gas venting to occur 1 or 2 ms earlier. After this point, the observed rate of pressure rise and peak pressure are both reproduced by the predictions at the ignition end of the vessel, with the overall duration of the pressure pulse being only slightly overpredicted. At the vent end of the vessel, the rate of pressure rise and pulse duration are again predicted well, although there is some underestimation of the peak overpressure attained at this position. At both positions the timing of the peak pressure, associated with the completion of rapid combustion behind the first obstacle, is predicted with reasonable accuracy, although pressure pulses and reflections within the vessel caused by the ignition of regions of highly turbulent unburned gas do lead to predicted profiles that exhibit more fluctuations than are observed. In line with previous comments, the overprediction in the rate of pressure decay at the ignition end of the vessel, and the underestimation of peak pressures occurring at the vent end, are most likely caused by inaccurate modeling of pressures generated external to the vessel. This is consistent with earlier findings [9] where the decay of predicted axial velocities within this vessel was also found to be too rapid.

Overall, the comparisons between measurements and predictions demonstrate that the mathematical model provides a reasonable simulation of combustion within cylindrical vessels that contain turbulence-inducing obstacles of the type investigated. In particular, good agreement with observations is obtained for flame speed and shape, with the dynamics of the various combustion processes occurring in the

different chambers of the vessels being reproduced. The rate at which combustion occurs in the various chambers is also well predicted, with rapid turbulent combustion in the shear layers and recirculation zones induced by obstacles, responsible for pressure generation, being predicted with sufficient accuracy to yield reasonable values for the overpressures. In addition, results obtained in empty and obstacle-containing enclosures demonstrate that, provided obstacle-generated turbulence occurs sufficiently early in the computations, this modeling approach allows the transition from laminar to turbulent flame propagation which occurs in many explosion situations to be accommodated.

Earlier applications [5] of the present model have also demonstrated its ability to predict reliably explosions in much larger enclosures, and in particular in a 10-m-long, 2.5-m-diameter, cylindrical vessel which contained five orifice plates, each with an area blockage of 30%. Turbulence-enhanced burning within the latter vessel was predicted to reach maximum local values of $u_t/u_l = 23$, $Re_l = 10^4$, and $K > 0.9$. Taken together with the present results, these studies have demonstrated the ability of the model to predict explosions in vessels at widely disparate scales, and, as might be anticipated, that the overall accuracy of the model improves as turbulence generated by flow ahead of the flame increases to levels where the turbulence modeling approach adopted can be considered to be valid.

CONCLUSIONS

An experimental and theoretical study of premixed flame propagation in small-scale, cylindrical vessels has been described. Data gathered in an empty vessel and obstacle-containing enclosures have been used to elucidate the dynamics of the various combustion processes occurring in the different chambers of the vessels, with laser sheet images used to further understanding of the turbulent premixed combustion process. Flame propagation through the vessels, up until flame venting, was found to be substantially laminar, with significant overpressure only being generated in the later stages of explosions due to rapid turbulent combustion in the shear layers and recirculation zones induced by the obstacles.

The experimental data generated have been used to assess the accuracy of a mathematical model of explosions based on solutions to the fluid flow equations and using a semi-empirical approach to modeling the turbulent premixed combustion process. Overall, comparisons between measurements and predictions demonstrate that the model provides a reasonable simulation of combustion within obstacle-containing enclosures of the type investigated, with the model providing reasonable values for the overpressures generated. Comparisons have also demonstrated that provided obstacle-generated turbulence occurs sufficiently early in the computations, the modeling approach adopted accommodates the transition from laminar to turbulent flame propagation which occurs in many explosion situations.

Further work remains to be performed, and in particular there is a requirement for detailed experimental data in the highly turbulent shear layers and recirculation zones of the flow in order to allow a more quantitative assessment of the turbulent premixed combustion model. In addition, improvements in the accuracy with which the combustion process external to the vessel is modeled are required.

The authors thank H. Jaggers for his assistance in performing the experimental work. The calculations reported in this paper were made using a modified version of the Mantis Numerics Ltd. code, COBRA. This paper is published by permission of BG Technology.

REFERENCES

1. Moen, I. O., Donato, M., Knystautas, R., and Lee, J. H. S., *Combust. Flame* 39:21–32 (1980).
2. Lindstedt, R. P., and Sakthitharan, V., *Ninth Symposium on Turbulent Shear Flows*, Springer-Verlag, Berlin, 1993, pp. 389–409.
3. Hjertager, B. H., *Combust. Sci. Technol.* 27:159–170 (1982).
4. Lindstedt, R. P., and Sakthitharan, V., *Eighth Symposium on Turbulent Shear Flows*, Technical University of Munich, 9–11 September 1991.
5. Catlin, C. A., Fairweather, M., and Ibrahim, S. S., *Combust. Flame* 102:115–128 (1995).

6. Starke, R., and Roth, P., *Combust. Flame* 75:111–121 (1989).
7. Phylaktou, H., and Andrews, G. E., *Combust. Flame* 85:363–379 (1991).
8. Pu, Y. K., Mazurkiewicz, J., Jarosinski, J., and Kauffman, C. W., *Twenty-Second Symposium (International) on Combustion*, The Combustion Institute, Pittsburgh, 1988, pp. 1789–1797.
9. Fairweather, M., Ibrahim, S. S., Jaggers, H., and Walker, D. G., *Twenty-Sixth Symposium (International) on Combustion*, The Combustion Institute, Pittsburgh, 1996, pp. 365–371.
10. Gosman, A. D., in *The Thermodynamics and Gas Dynamics of Internal-Combustion Engines, Vol. 2* (J. H. Horlock and D. E. Winterbone, Eds.), Clarendon Press, Oxford, 1986, pp. 616–772.
11. Jones, W. P., and Whitelaw, J. H., *Combust. Flame* 48:1–26 (1982).
12. Jones, W. P., in *Prediction Methods for Turbulent Flows* (W. Kollmann, Ed.), Hemisphere, New York, 1980, pp. 379–421.
13. Catlin, C. A., and Lindstedt, R. P., *Combust. Flame* 85:427–439 (1991).
14. Zel'dovich, Y. B., *Combust. Flame* 39:219–224 (1980).
15. Gülder, O. L., *Twenty-Third Symposium (International) on Combustion*, The Combustion Institute, Pittsburgh, 1990, pp. 743–750.
16. Bray, K. N. C., *Proc. R. Soc. Lond. A* 431:315–335 (1990).
17. Poinsot, T., Veynante, D., and Candel, S., *J. Fluid Mech.* 228:561–606 (1991).
18. Barr, P. K., *Combust. Flame* 82:111–125 (1990).
19. Abdel-Gayed, R. G., Bradley, D., and Lawes, M., *Proc. R. Soc. Lond. A* 414:389–413 (1987).

Received 25 April 1997; accepted 5 April 1998